Electronic Supplementary Material (ESI) for Physical Chemistry Chemical Physics.

Enhancement of weak ferromagnetism, exotic structure prediction and diverse electronic properties in holmium substituted multiferroic bismuth ferrite

Maria Čebela[1,2,3*], Dejan Zagorac[2,3*], Igor Popov[4,5*], Filip Torić[1], Teodoro Klaser[6], Željko Skoko[1], Damir Pajić[1*]

[1] University of Zagreb, Faculty of Science, Department of Physics, Bijenička cesta 32, 10000 Zagreb, Croatia

[2] Materials Science Laboratory, Institute of Nuclear Sciences Vinča, University of Belgrade, National Institute of the Republic of Serbia, Mike Petrovića Alasa 12-14, Belgrade, Serbia

[3] Center of Excellence "CextremeLab", Institute of Nuclear Sciences Vinča, University of Belgrade, National Institute of the Republic of Serbia, Mike Petrovića Alasa 12-14, Belgrade, Serbia

[4] Institute for Multidisciplinary Research, University of Belgrade, Kneza Višeslava 1, 11030 Belgrade, Serbia

[5] Institute of Physics, University of Belgrade, Pregrevica 118, 11080 Belgrade, Serbia

[6] Ruđer Bošković Institute, Bijenička cesta 54, 10000 Zagreb, Croatia

Corresponding Authors: mcebela@vinca.rs , dzagorac@vinca.rs , popov@ipb.ac.rs , dpajic@phy.hr

Supporting Information

Supporting Tables

Table S1. Structural parameters of the samples doped with 2%, 5% and 10% Ho studied by powder X-ray diffraction and the data were refined by the Rietveld method.

	BHFO-2	BHFO-5	BHFO-10
Empirical formula	$Bi_{5.88}Ho_{0.12}Fe_6O_{12}$	$Bi_{5.70}Ho_{0.30}Fe_6O_{12}$	$Bi_{5.40}Ho_{0.60}Fe_6O_{12}$
Crystal system	Trigonal (hexagonal axes)	Trigonal (hexagonal axes)	Trigonal (hexagonal axes)
Space group	*R3c*	*R3c*	*R3c*
a/Å	5.6082(7)	5.5870(6)	5.5800(7)
c/Å	13.9253(9)	13.8873(8)	13.8739(8)
Agreement parameters			
R_{wp}/%	10.3	14.1	11.2
R_p/%	8.1	11.9	9.8
R_{exp}/%	7.1	10.2	8.1
Refined atomic coordinates			
O (x)	0.438(3)	0.441(3)	0.445(3)
(y)	0.016(2)	0.015(2)	0.019(3)
(z)	0.948(5)	0.943(4)	0.951(5)
Bi/Ho (z)	0.223(1)	0.228(2)	0.226(1)

Table S2. Calculated values of the global instability index (GII) and tilt system of the most promising $Bi_{0.98}Ho_{0.02}FeO_3$ modifications using the bond valence (BVC) method.

Modification	Space group	Tilt system	GII
β-$Bi_{0.98}Ho_{0.02}FeO_3$	*Pnma*	$a^-b^+a^-$	0.03816
R-$Bi_{0.98}Ho_{0.02}FeO_3$	*R*-3*c*	$a^-a^-a^-$	0.04284
T_1-$Bi_{0.98}Ho_{0.02}FeO_3$	*P*4/*mbm*	a^0a^0c-	0.08938
T_2-$Bi_{0.98}Ho_{0.02}FeO_3$	*I*4/*mcm*	a^0a^0c-	0.08938
γ-$Bi_{0.98}Ho_{0.02}FeO_3$	*Pm*-3*m*	$a^0a^0a^0$	0.72910

Table S3. Structural data of the most promising $Bi_{0.98}Ho_{0.02}FeO_3$ perovskite modifications calculated using the BVC method.

Modification, space group and Wyckoff position	**Cell parameters(Å), unit-cell volume (Å^3) and fractional coordinates**
β-$Bi_{0.98}Ho_{0.02}FeO_3$	*a*=5.60, *b*=7.76, *c*=5.39
Pnma(62)	*V*=234.55
Bi 4*c*	0.5599 1/4 0.5207
Ho 4*c*	0.5599 1/4 0.5207
Fe 4*b*	1/2 0 0
O1 4*c*	-0.0181 1/4 0.4013
O2 8*d*	0.2958 0.0494 0.7006
R-$Bi_{0.98}Ho_{0.02}FeO_3$	*a*=5.44, *c*=13.96
$R\bar{3}c$(167)	*V*=357.56
Bi 6*a*	0 0 ¼
Ho 6*a*	0 0 ¼
Fe1 6*b*	2/3 1/3 1/3
O 18*e*	0.4091 0 1/4
T_1-$Bi_{0.98}Ho_{0.02}FeO_3$	*a*=5.36, *c*=4.03
P4/mbm (127)	V=115.73
Bi 2*c*	0 1/2 ½
Ho 2*c*	0 1/2 1/2
Fe 2*a*	0 0 0
O1 2*b*	0 0 1/2

O2 4*g*	0.1592 0.6592 0
T_2-$Bi_{0.98}Ho_{0.02}FeO_3$ *I4/mcm*(140) Bi 4*b* Ho 4*b* Fe 4*c* O1 4*a* O2 8*h*	*a*=5.36, *c*=8.06 *V*=231.45 0 1/2 1/4 0 1/2 1/4 0 0 0 0 0 1/4 0.3408 0.8408 0
γ-$Bi_{0.98}Ho_{0.02}FeO_3$ *Pm*-3*m*(221) Bi 1*b* Ho 1*b* Fe 1*a* O 3*d*	*a*=4.03 *V*=65.50 1/2 1/2 1/2 1/2 1/2 1/2 0 0 0 0 0 1/2

Table S4. Calculated values of the global instability index (GII) and tilt system of the most promising $Bi_{0.95}Ho_{0.05}FeO_3$ modifications using the bond valence (BVC) method.

Modification	Space group	Tilt system	GII
β-$Bi_{0.95}Ho_{0.05}FeO_3$	*Pnma*	$a^-b^+a^-$	0.05815
R-$Bi_{0.95}Ho_{0.05}FeO_3$	*R*-3*c*	$a^-a^-a^-$	0.06113
T_1-$Bi_{0.95}Ho_{0.05}FeO_3$	*P*4/*mbm*	a^0a^0c-	0.09992
T_2-$Bi_{0.95}Ho_{0.05}FeO_3$	*I*4/*mcm*	a^0a^0c-	0.09992
γ-$Bi_{0.95}Ho_{0.05}FeO_3$	*Pm*-3*m*	$a^0a^0a^0$	0.73225

Table S5. Structural data of the most promising $Bi_{0.95}Ho_{0.05}FeO_3$ perovskite modifications calculated using the BVC method.

Modification, space group and Wyckoff position	**Cell parameters(Å), unit-cell volume (Å^3) and fractional coordinates**
β-$Bi_{0.95}Ho_{0.05}FeO_3$ *Pnma*(62) Bi 4*c* Ho 4*c* Fe 4*b* O1 4*c* O2 8*d*	*a*=5.59, *b*=7.76, *c*=5.39 *V*=234.33 0.5604 1/4 0.5209 0.5604 1/4 0.5209 1/2 0 0 -0.0182 1/4 0.4008 0.2960 0.0496 0.7004

R-$Bi_{0.95}Ho_{0.05}FeO_3$	*a*=5.44, *c*=13.96
R-3*c*(167)	*V*=357.36
Bi 6*a*	0 0 ¼
Ho 6*a*	0 0 1/4
Fe1 6*b*	2/3 1/3 1/3
O 18*e*	0.5911 0 1/4
T_1-$Bi_{0.95}Ho_{0.05}FeO_3$	*a*=5.36, *c*=4.03
P4/mbm (127)	V=115.63
Bi 2*c*	0 1/2 1/2
Ho 2*c*	0 1/2 1/2
Fe 2*a*	0 0 0
O1 2*b*	0 0 1/2
O2 4*g*	0.1589 0.6589 0
T_2-$Bi_{0.95}Ho_{0.05}FeO_3$	*a*=5.36, *c*=8.06
I4/mcm(140)	*V*=231.25
Bi 4*b*	0 1/2 1/4
Ho 4*b*	0 1/2 1/4
Fe 4*c*	0 0 0
O1 4*a*	0 0 1/4
O2 8*h*	0.3411 0.8411 0
γ-$Bi_{0.95}Ho_{0.05}FeO_3$	*a*=4.03
Pm-3*m*(221)	*V*=65.50
Bi 1*b*	1/2 1/2 1/2
Ho 1*b*	1/2 1/2 1/2
Fe 1*a*	0 0 0
O 3*d*	0 0 1/2

Table S6. Calculated values of the global instability index (GII) and tilt system of the most promising $Bi_{0.9}Ho_{0.1}FeO_3$ modifications using the bond valence (BVC) method.

Modification	Space group	Tilt system	GII
β-$Bi_{0.9}Ho_{0.1}FeO_3$	*Pnma*	$a^-b^+a^-$	0.08023
R-$Bi_{0.9}Ho_{0.1}FeO_3$	*R*-3*c*	$a^-a^-a^-$	0.08226
T_1-$Bi_{0.9}Ho_{0.1}FeO_3$	*P*4/*mbm*	a^0a^0c-	0.11480
T_2-$Bi_{0.9}Ho_{0.1}FeO_3$	*I*4/*mcm*	a^0a^0c-	0.11480
γ-$Bi_{0.9}Ho_{0.1}FeO_3$	*Pm*-3*m*	$a^0a^0a^0$	0.73746

Table S7. Structural data of the most promising $Bi_{0.9}Ho_{0.1}FeO_3$ perovskite modifications calculated using the BVC method.

Modification, space group and Wyckoff position	**Cell parameters(Å), unit-cell volume (Å^3) and fractional coordinates**
β-$Bi_{0.9}Ho_{0.1}FeO_3$	*a*=5.60, *b*=7.76, *c*=5.39
Pnma(62)	*V*=233.93
Bi 4*c*	0.5613 1/4 0.5212
Ho 4*c*	0.5613 1/4 0.5212
Fe 4*b*	1/2 0 0
O1 4*c*	-0.0185 1/4 0.4000
O2 8*d*	0.2963 0.0500 0.7000
R-$Bi_{0.9}Ho_{0.1}FeO_3$	*a*=5.43, *c*=13.96
R-3*c*(167)	*V*=357.05
Bi 6*a*	0 0 1/4
Ho 6*a*	0 0 1/4
Fe1 6*b*	2/3 1/3 1/3
O 18*e*	0.5916 0 1/4
T_1-$Bi_{0.9}Ho_{0.1}FeO_3$	*a*=5.35, *c*=4.03
P4/mbm (127)	*V*=115.45
Bi 2*c*	0 1/2 1/2
Ho 2*c*	0 1/2 1/2
Fe 2*a*	0 0 0
O1 2*b*	0 0 1/2
O2 4*g*	0.1583 0.6583 0
T_2-$Bi_{0.9}Ho_{0.1}FeO_3$	*a*=5.35, *c*=8.06
I4/mcm (140)	*V*=230.91
Bi 4*b*	0 1/2 1/4
Ho 4*b*	0 1/2 1/4
Fe 4*c*	0 0 0
O1 4*a*	0 0 1/4
O2 8*h*	0.3417 0.8417 0
γ-$Bi_{0.9}Ho_{0.1}FeO_3$	*a*=4.03
Pm-3*m* (221)	*V*=65.50
Bi 1*b*	1/2 1/2 1/2
Ho 1*b*	1/2 1/2 1/2
Fe 1*a*	0 0 0
O 3*d*	0 0 1/2

Supporting Figures

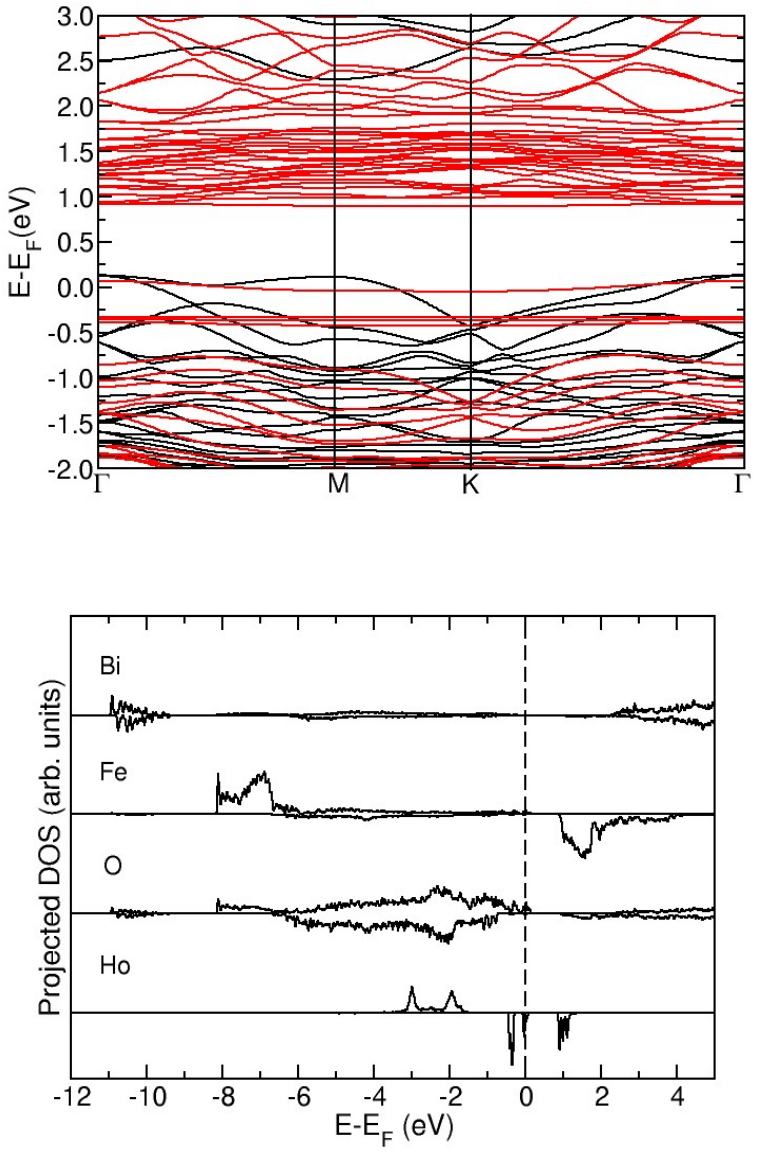

Figure S1. Electro-magnetic properties of the half-metallic **alpha FM** structure: a) Band structure along lines between high symmetry points. Black lines present spin-up and red line spin-down bands; b) Element-resolved density of states (DOS). Mirrored graphs correspond to spin-up and spin-down states. Alpha FM has a relatively small gap of ~0.9 eV with an asymmetry of dispersion of valence (large dispersion) and conduction (small dispersion, flat band). Suitable for. e.g. application as a switch.

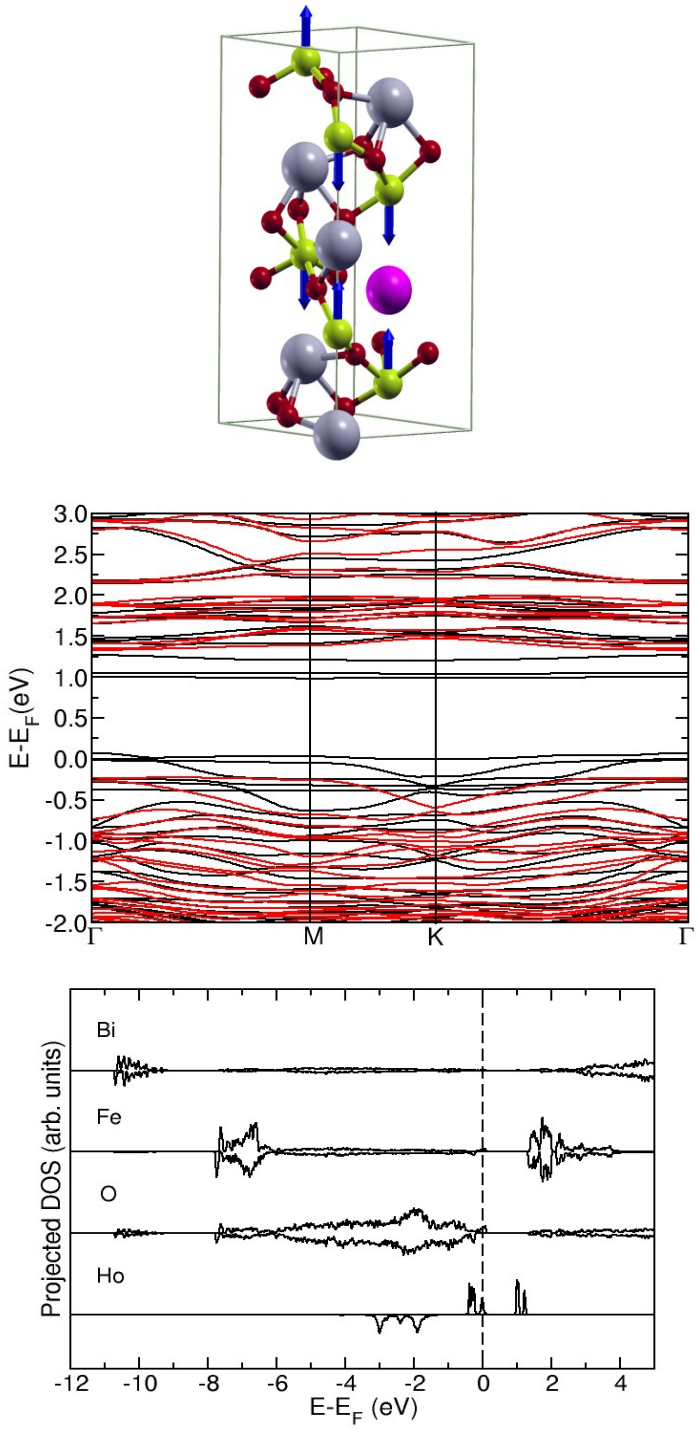

Figure S2. Electro-magnetic properties of the half-metallic **alpha AFM1** structure: a) Calculation cell with spin texture marked by the blue arrows; b) Band structure along lines between high symmetry points. Black lines present spin-up and red line spin-down bands; c) Element-resolved density of states (DOS). Mirrored graphs correspond to spin-up and spin-down states.

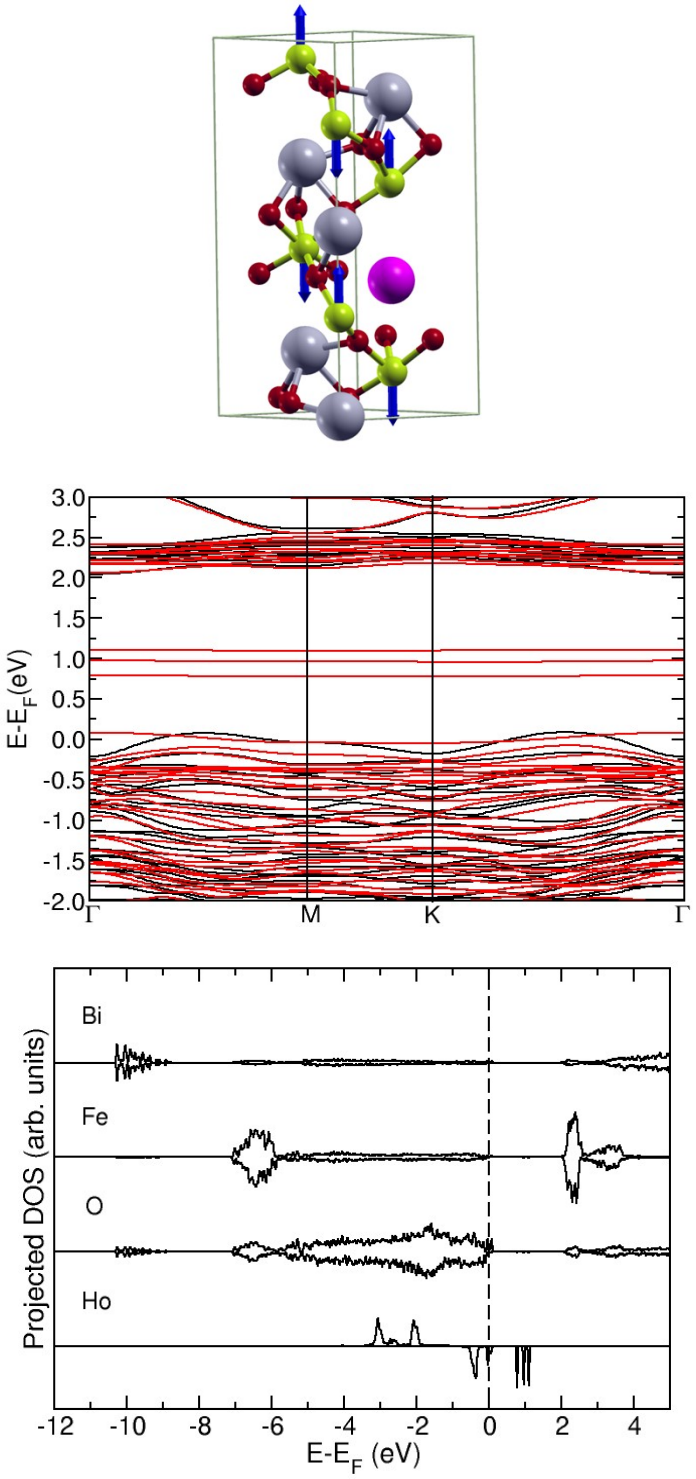

Figure S3. Electro-magnetic properties of the **alpha AFM2** structure: a) Calculation cell with spin texture marked by the blue arrows; b) Band structure along lines between high symmetry points. Black lines present spin-up and red line spin-down bands; c) Element-resolved density of states (DOS). Mirrored graphs correspond to spin-up and spin-down states.

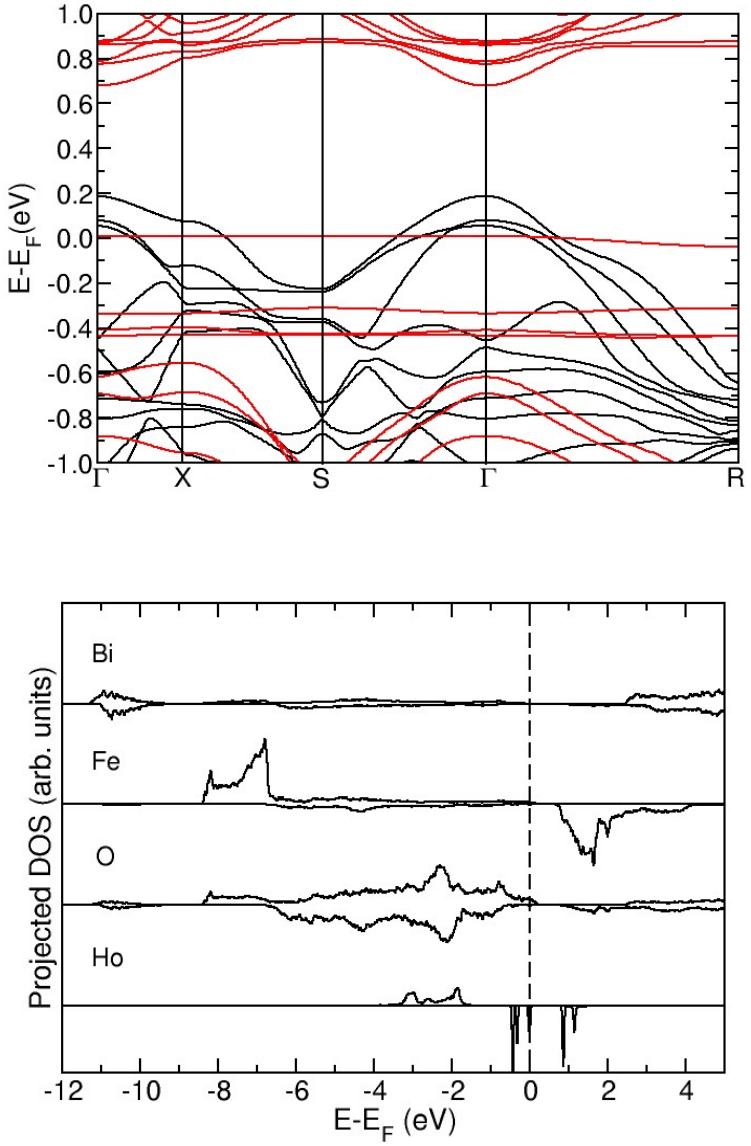

Figure S4. Electro-magnetic properties of the half-metallic **beta FM** structure: a) Band structure along lines between high symmetry points. Black lines present spin-up and red line spin-down bands; b) Element-resolved density of states (DOS). Mirrored graphs correspond to spin-up and spin-down states.

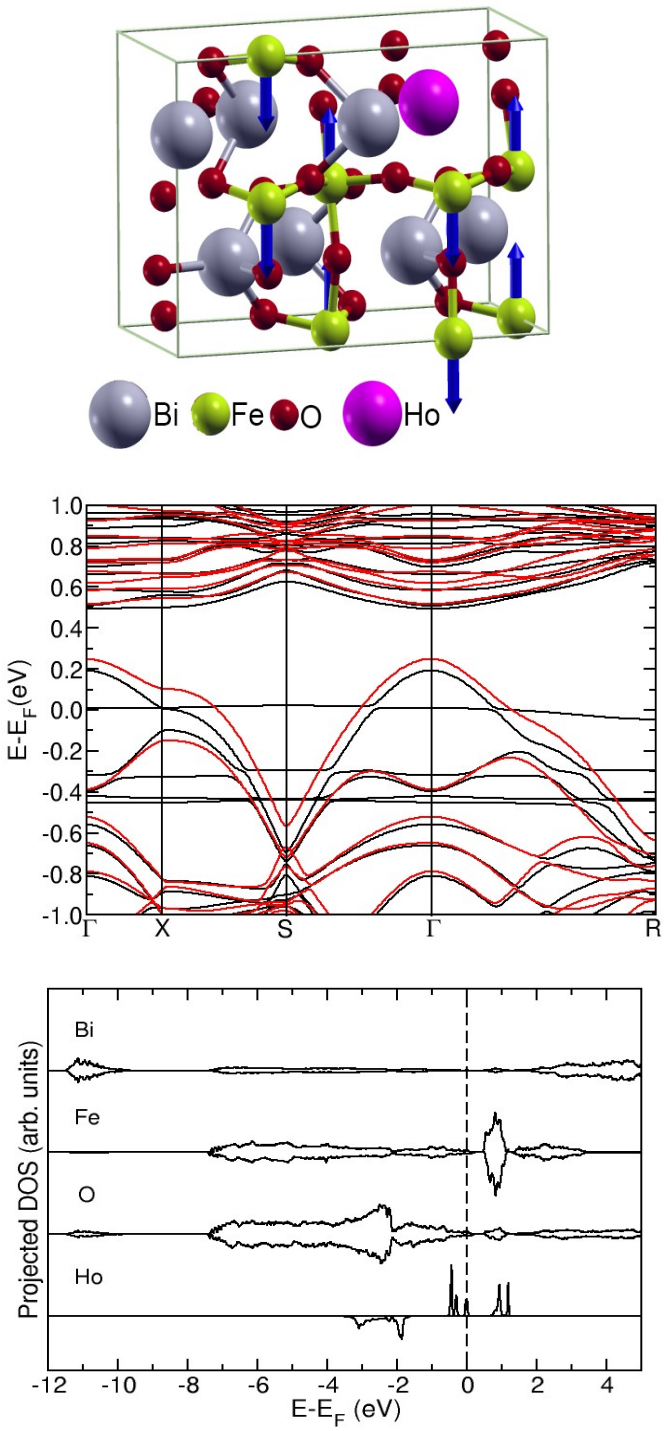

Figure S5. Electro-magnetic properties of the **beta AFM1** structure: a) Calculation cell with spin texture marked by the blue arrows; b) Band structure along lines between high symmetry points. Black lines present spin-up and red line spin-down bands; c) Element-resolved density of states (DOS). Mirrored graphs correspond to spin-up and spin-down states. Beta AFM1 has a dispersive valence band while the conduction band has a relatively small dispersion. This finding together with the small band gap indicates that beta AFM1 is suitable for application as a switch.

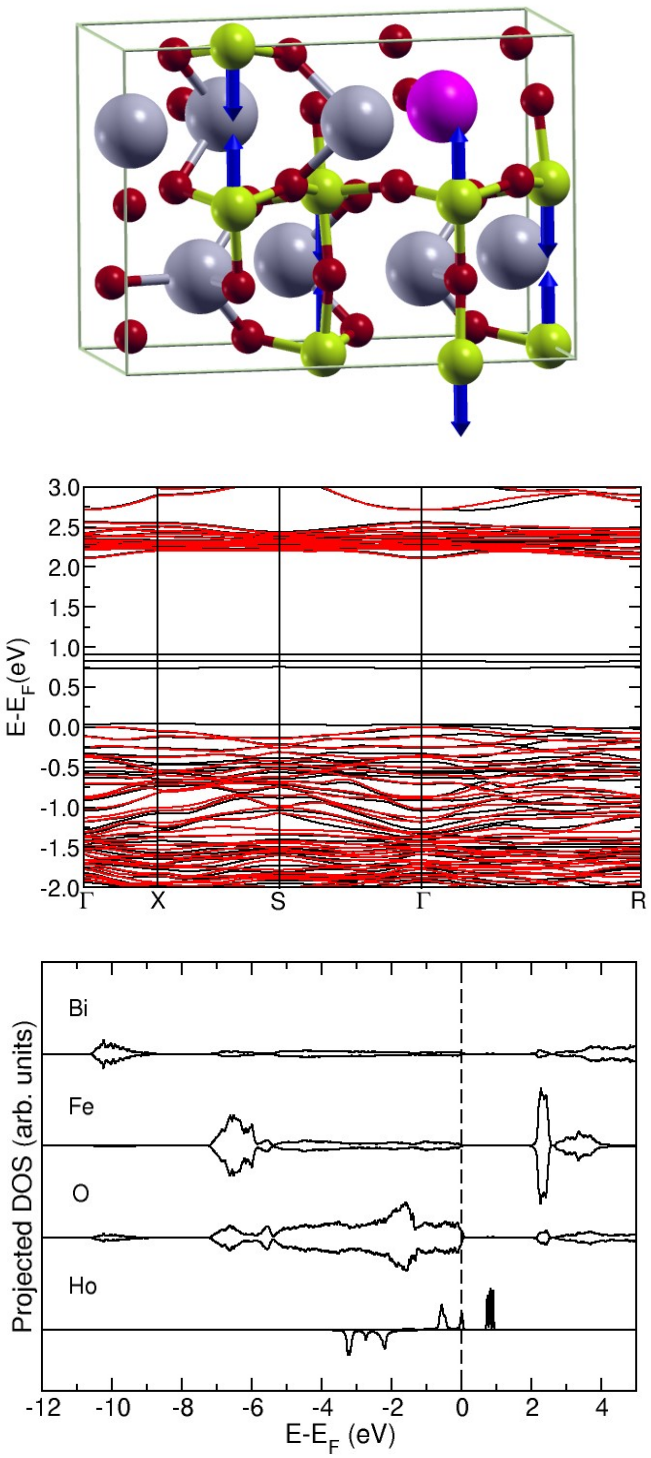

Figure S6. Electro-magnetic properties of the **beta AFM2** structure: a) Calculation cell with spin texture marked by the blue arrows; b) Band structure along lines between high symmetry points. Black lines present spin-up and red line spin-down bands; c) Element-resolved density of states (DOS). Mirrored graphs correspond to spin-up and spin-down states. Both beta AFM1 and AFM2 structures appear as semiconductors with beta AFM1 direct band gap of 0.2-1.70 eV and dispersion

of 1.70 eV, while beta AFM2 type shows a direct band gap of 2 eV and dispersion of valence bands of only 0.15 eV (Table 2 and supporting Figures).

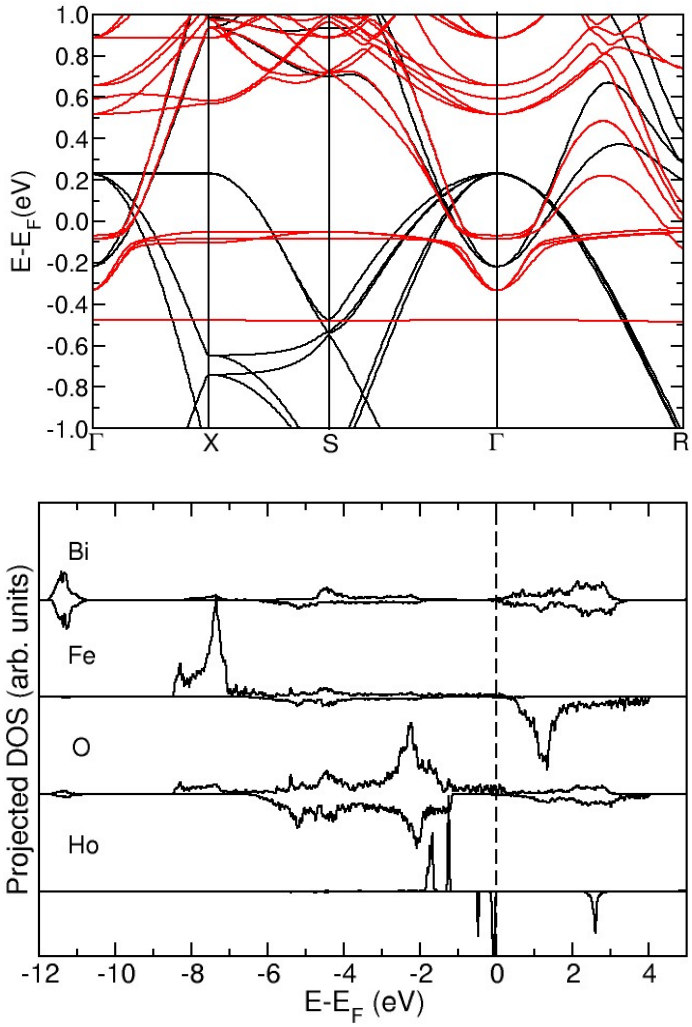

Figure S7. Electro-magnetic properties of the **gamma FM** structure: a) Band structure along lines between high symmetry points. Black lines present spin-up and red line spin-down bands; b) Element-resolved density of states (DOS). Mirrored graphs correspond to spin-up and spin-down states.

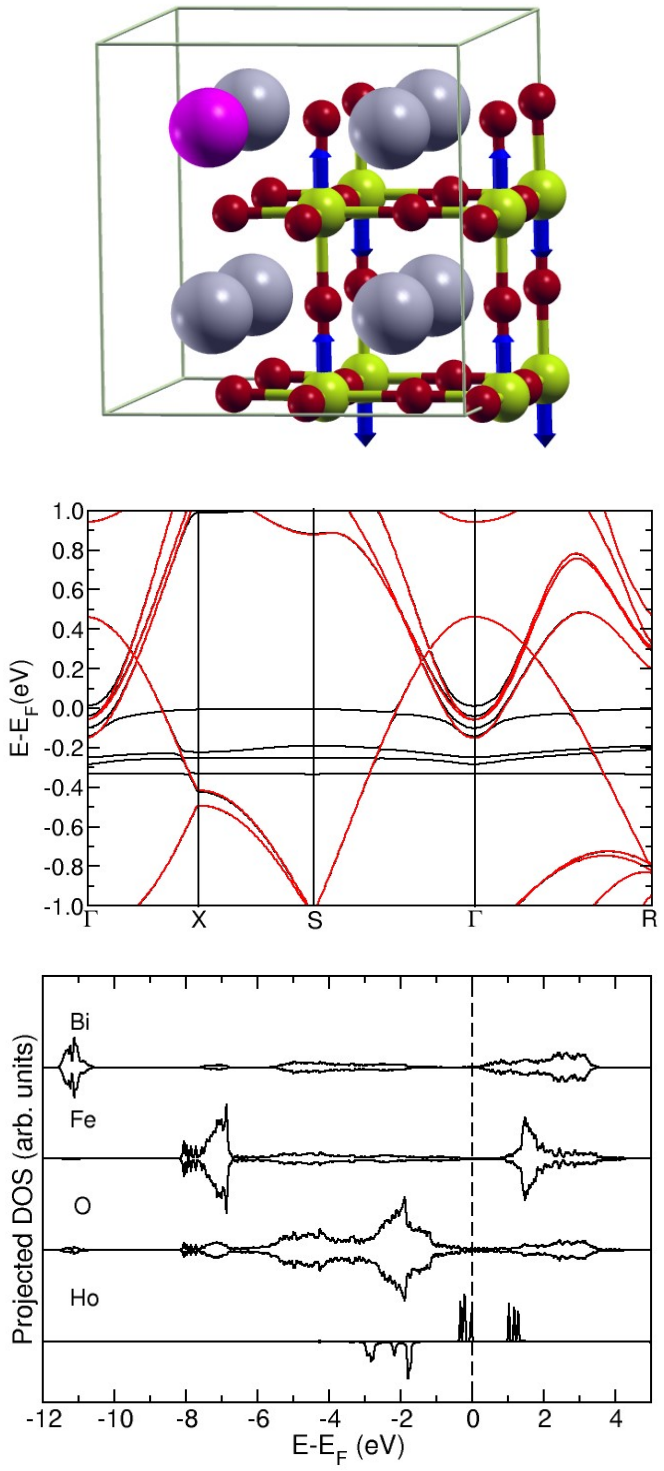

Figure S8. Electro-magnetic properties of the semimetallic **gamma AFM1** structure: a) Calculation cell with spin texture marked by the blue arrows; b) Band structure along lines between high symmetry points. Black lines present spin-up and red line spin-down bands; c) Element-resolved density of states (DOS). Mirrored graphs correspond to spin-up and spin-down states.

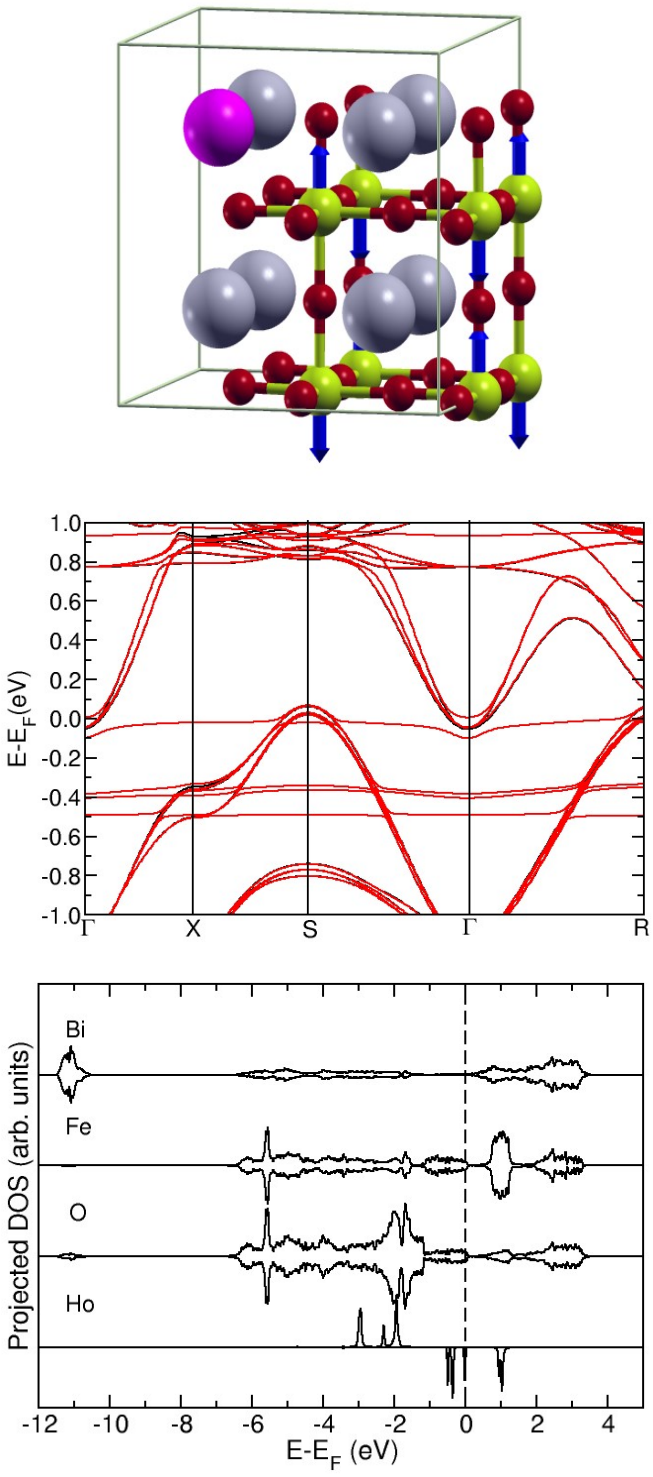

Figure S9. Electro-magnetic properties of the semimetallic **gamma AFM2** structure: a) Calculation cell with spin texture marked by the blue arrows; b) Band structure along lines between high symmetry points. Black lines present spin-up and red line spin-down bands; c) Element-resolved density of states (DOS). Mirrored graphs correspond to spin-up and spin-down states.

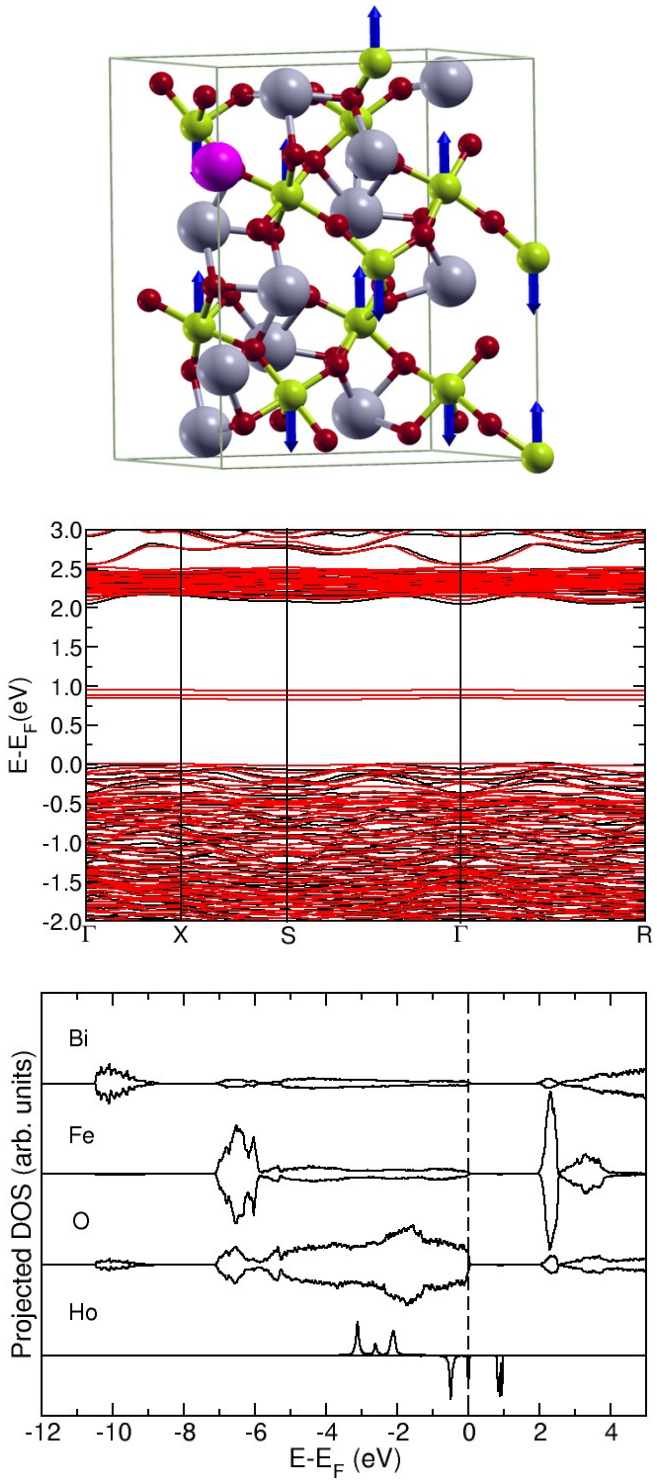

Figure S9. Electro-magnetic properties of the **R-type AFM1** structure: a) Calculation cell with spin texture marked by the blue arrows; b) Band structure along lines between high symmetry points. Black lines present spin-up and red line spin-down bands; c) Element-resolved density of states (DOS). Mirrored graphs correspond to spin-up and spin-down states.

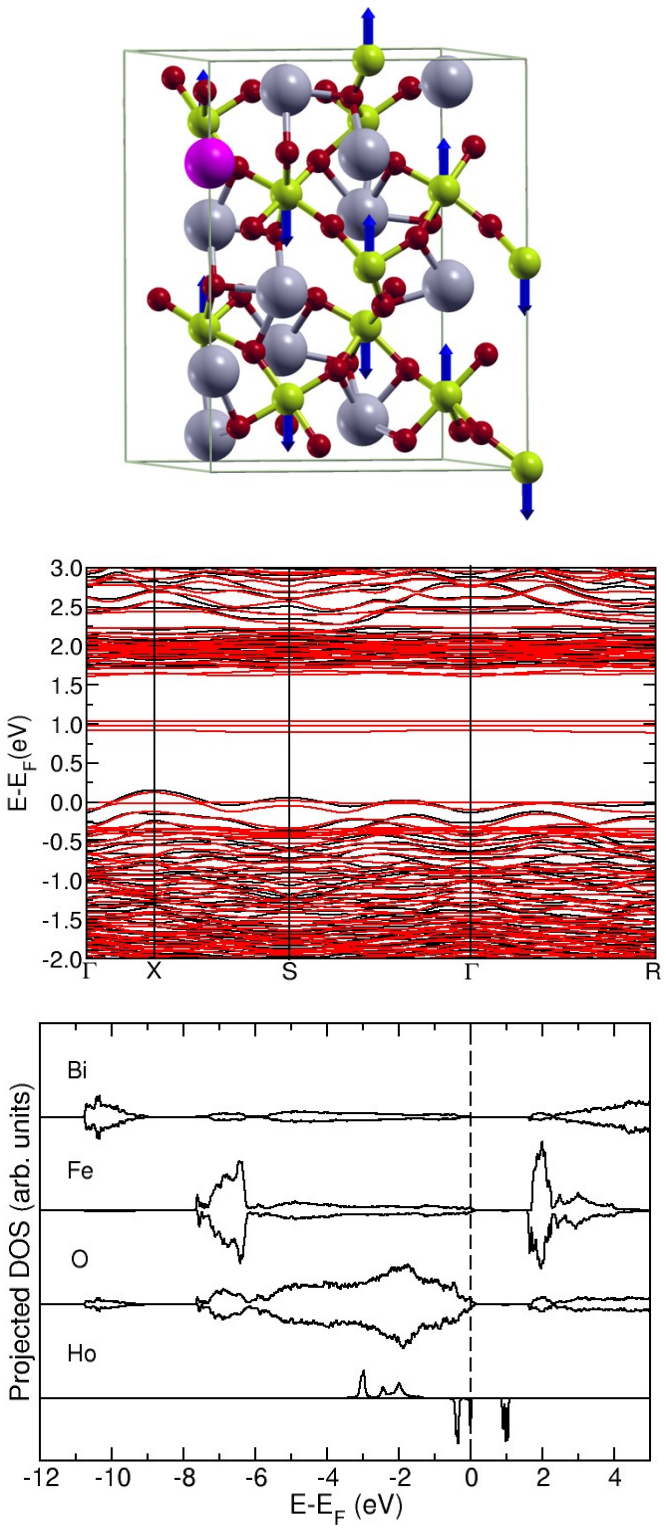

Figure S10. Electro-magnetic properties of the **R-type AFM2** structure: a) Calculation cell with spin texture marked by the blue arrows; b) Band structure along lines between high symmetry points. Black lines present spin-up and red line spin-down bands; c) Element-resolved density of states (DOS). Mirrored graphs correspond to spin-up and spin-down states.

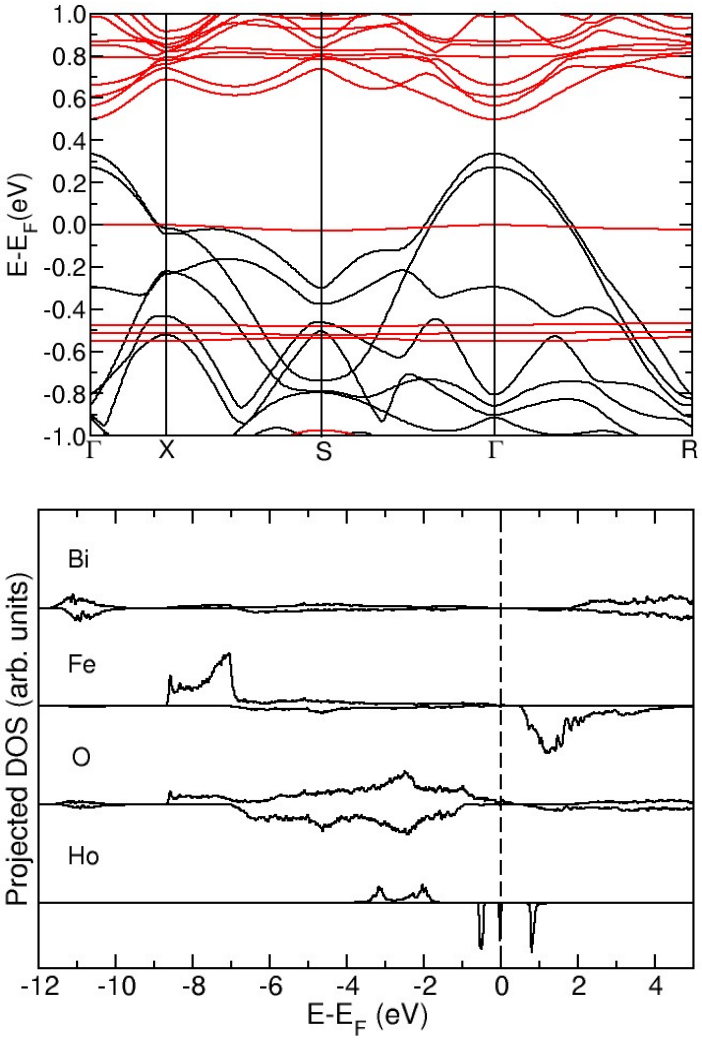

Figure S11. Electro-magnetic properties of the half-metallic **T1-type FM** structure: a) Band structure along lines between high symmetry points. Black lines present spin-up and red line spin-down bands; b) Element-resolved density of states (DOS). Mirrored graphs correspond to spin-up and spin-down states.

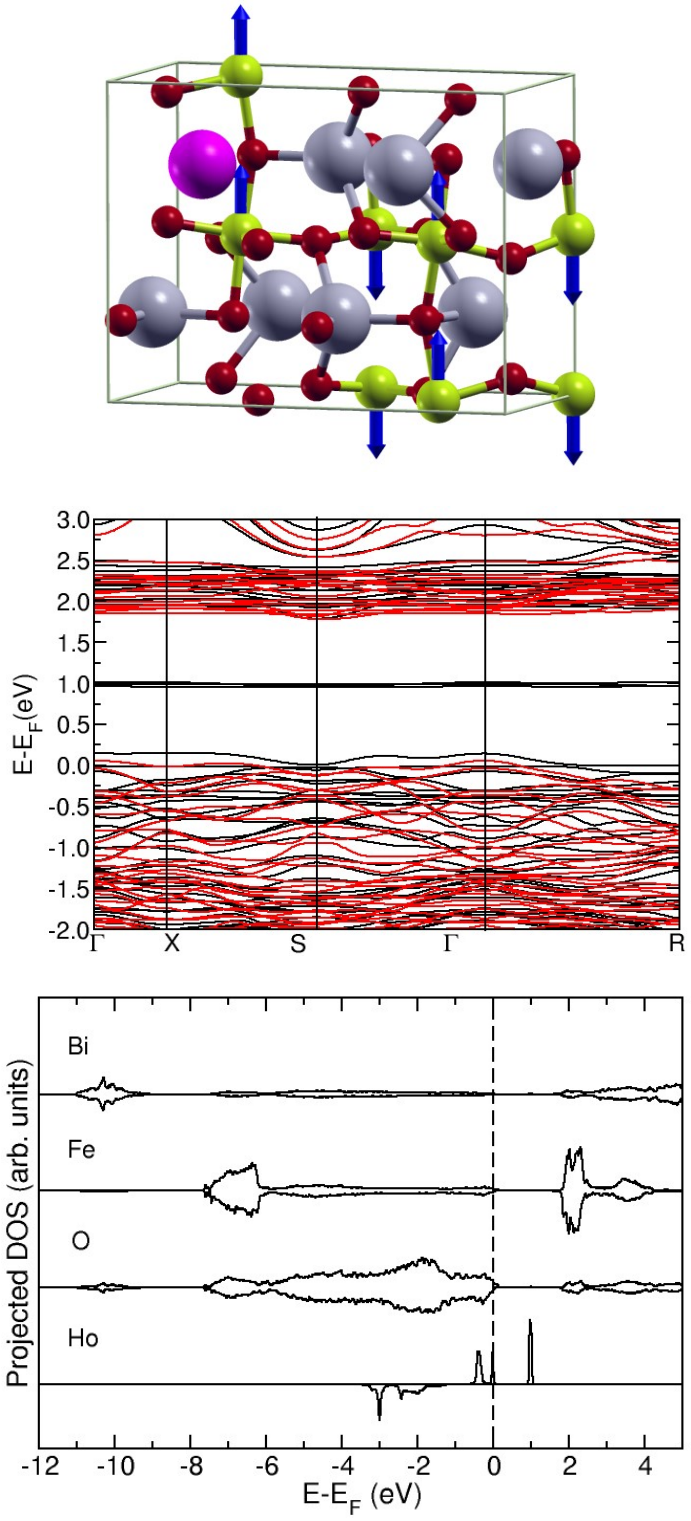

Figure S12. Electro-magnetic properties of the **T1-type AFM1** structure: a) Calculation cell with spin texture marked by the blue arrows; b) Band structure along lines between high symmetry points. Black lines present spin-up and red line spin-down bands; c) Element-resolved density of states (DOS). Mirrored graphs correspond to spin-up and spin-down states.

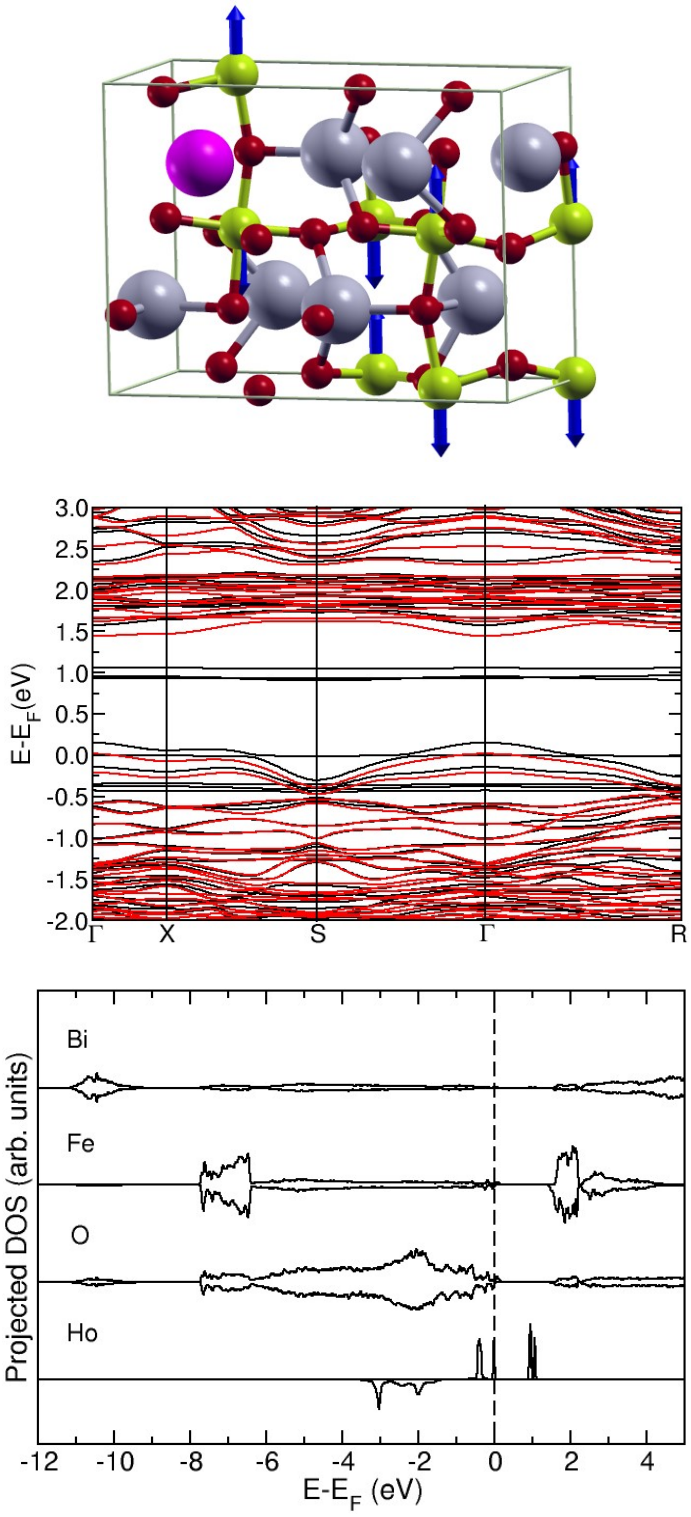

Figure S13. Electro-magnetic properties of the **T1-type AFM2** structure: a) Calculation cell with spin texture marked by the blue arrows; b) Band structure along lines between high symmetry points. Black lines present spin-up and red line spin-down bands; c) Element-resolved density of states (DOS). Mirrored graphs correspond to spin-up and spin-down states.

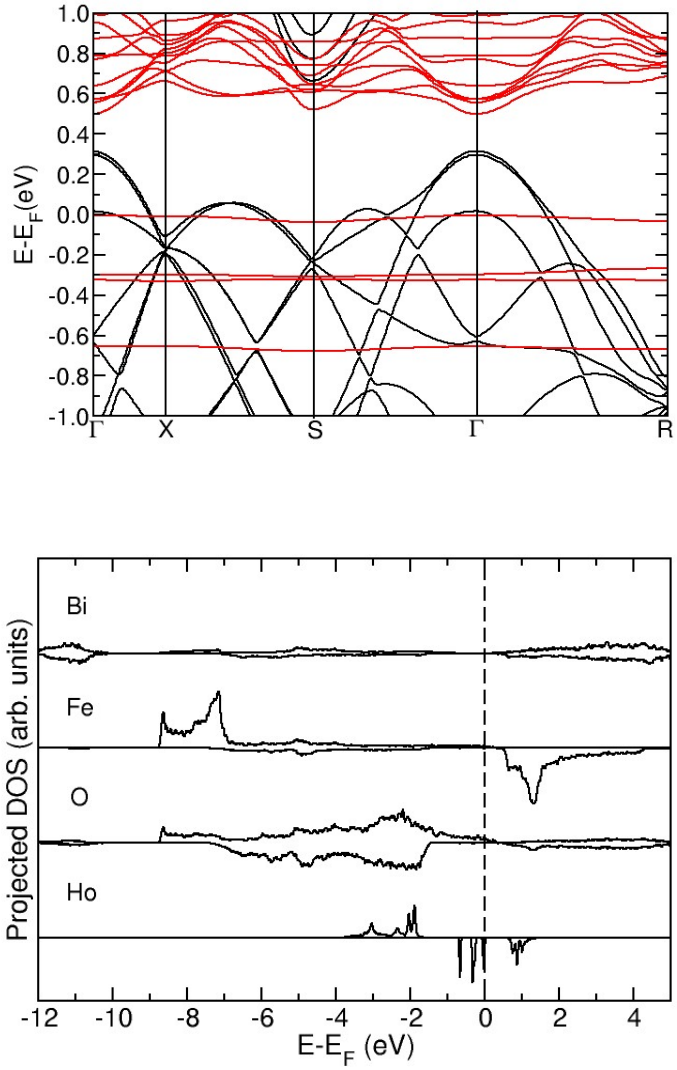

Figure S14. Electro-magnetic properties of the half-metallic **T2-type FM** structure: a) Band structure along lines between high symmetry points. Black lines present spin-up and red line spin-down bands; b) Element-resolved density of states (DOS). Mirrored graphs correspond to spin-up and spin-down states. T2 FM has a relatively large dispersion of the valence band and small dispersion of the conduction band, which is suitable for. e.g. application as a switch.

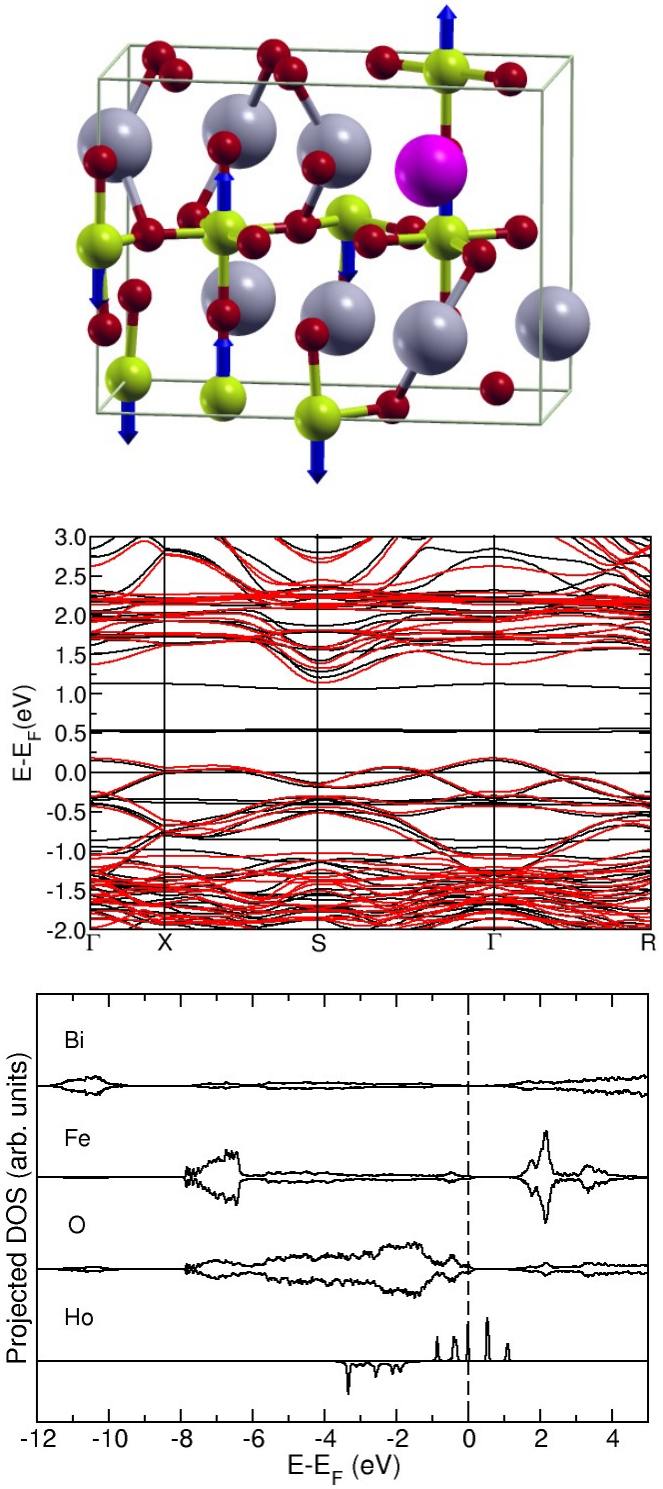

Figure S15. Electro-magnetic properties of the **T2-type AFM1** structure: a) Calculation cell with spin texture marked by the blue arrows; b) Band structure along lines between high symmetry points. Black lines present spin-up and red line spin-down bands; c) Element-resolved density of states (DOS). Mirrored graphs correspond to spin-up and spin-down states.

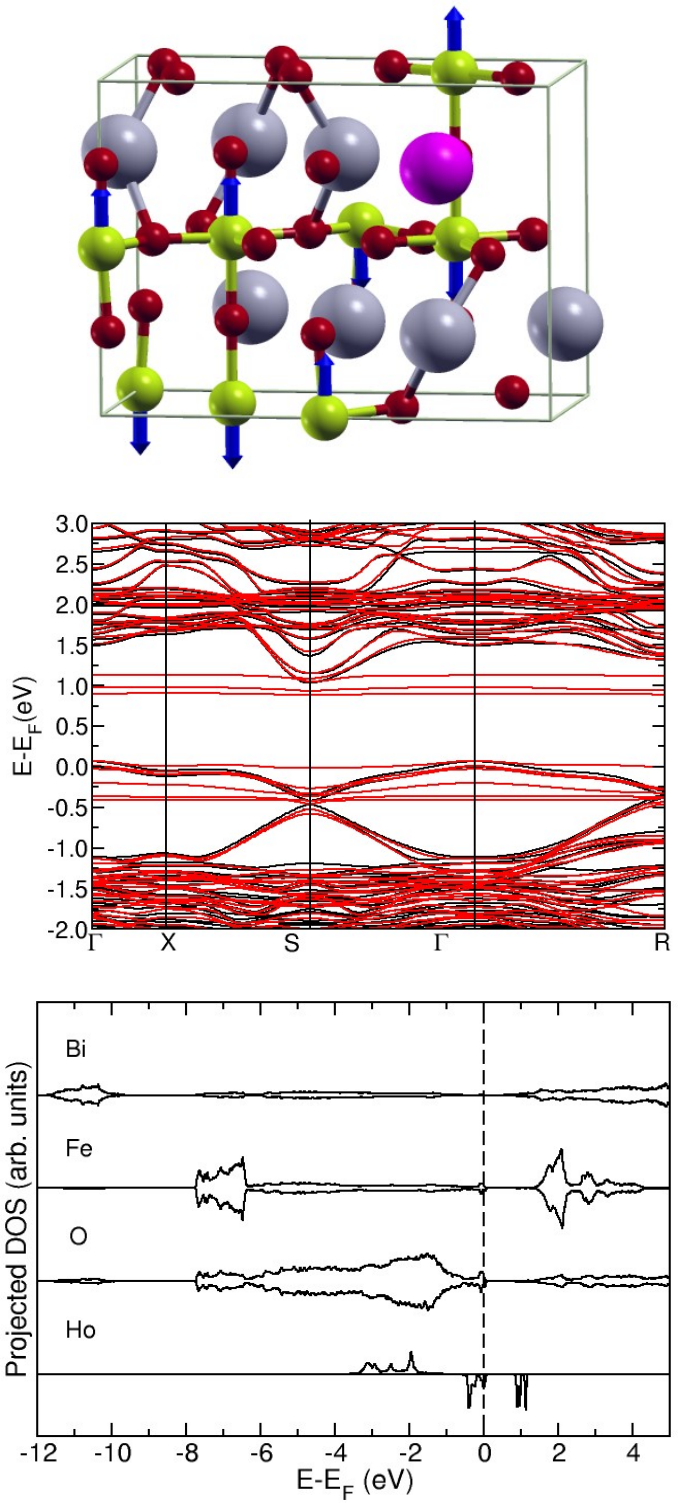

Figure S16. Electro-magnetic properties of the **T2-type AFM2** structure: a) Calculation cell with spin texture marked by the blue arrows; b) Band structure along lines between high symmetry points. Black lines present spin-up and red line spin-down bands; c) Element-resolved density of states (DOS). Mirrored graphs correspond to spin-up and spin-down states.